

Flow patterns and preferred sites of atherosclerotic lesions in the human aorta – II. Abdominal aorta

Shunsuke Endo ^{a,*}, Harry L. Goldsmith ^b and Takeshi Karino ^c

^a *Department of General Thoracic Surgery, Jichi Medical University, Tochigi, Japan*

^b *Department of Medicine, McGill University Health Centre, Montreal, QC, Canada*

^c *Research Institute for Electronic Science, Hokkaido University, Sapporo, Japan*

Received 5 February 2014

Accepted in revised form 21 August 2014

Abstract.

OBJECTIVE: As in Part I, to elucidate the role of fluid mechanical factors in the localized genesis and development of atherosclerotic lesions in man, here in the abdominal aorta.

METHODS: Flow patterns and preferred sites of atherosclerotic lesions in the aorta were studied in detail using the same isolated transparent aortic trees prepared from humans postmortem and the flow visualization and cinemicrographic techniques as in Part I.

RESULTS: Under steady flow simulating mid-systole, the flow was found to be disturbed at the aorto-celiac and aorto-superior mesenteric artery junctions by the formation of complex secondary and adverse flows along the lateral and posterior walls of the abdominal aorta. More complex secondary and adverse flows formed at the branching sites of the left and right renal arteries. Furthermore, considerable interactions occurred between the secondary and adverse flows formed at the branching sites of the above four arteries, resulting in the formation of a large and long recirculation zone along the lateral and posterior walls of the abdominal aorta corresponding to these branches. The velocity profile was almost flattened throughout the entire length of the descending aorta.

CONCLUSIONS: Atherosclerotic lesions were found mainly at the posterior and lateral walls of the abdominal aorta where slow adverse and recirculation flows formed and where wall shear stress was low.

Keywords: Aortic aneurysm, flow visualization, recirculation flow, secondary flow, velocity profile, wall shear stress

1. Introduction

It has been reported that the abdominal aorta is one of the most susceptible sites for atherogenesis in humans [1–5]. The problem of atherosclerosis in the abdominal aorta is the complication of atherosclerotic lesions with ulceration, intramural hemorrhage, and thrombosis. Furthermore, progressive degeneration of these lesions may change the property of the aortic wall and cause the formation of aneurysms with and without dissections of the vessel wall [6–8]. In fact, in an animal study with the monkey, it was shown that the formation of atherosclerotic plaques lead to aneurysmal enlargement

* Address for correspondence: Dr. Shunsuke Endo, Department of General Thoracic Surgery, Jichi Medical University, 1-3311 Yakushiji, Shimotsuke, Tochigi 329-0498, Japan. Tel.: +81 285 58 7368; Fax: +81 285 44 6271; E-mail: tcvshun@jichi.ac.jp.

of the aorta [9]. Pathological studies indicated that most of aortic aneurysms were based on extensive atherosclerotic lesions [5]. Atherosclerotic aneurysms were found mostly in the infra-renal abdominal aorta [5]. Atherosclerotic occlusive disease was often observed in the aortic sinus (coronary orifice) and at the iliac bifurcation [10].

Postmortem studies indicate that incipient atherosclerotic lesions in the human descending aorta develop not randomly, and not everywhere, but at particular sites such as the proximal lip of the orifice of major arteries branching off the descending aorta, and the posterior wall of the aorta [1–5]. Fluid mechanical factors are suspected to be involved in the localization of these atherosclerotic lesions. Therefore, extensive studies have been carried out in the past years on both the distribution of atherosclerotic lesions and the blood flow in this region as described in our previous paper [11]. In most cases, flow studies were focused on identifying the regions of high and low wall shear stresses (wall shear rates) by obtaining velocity distributions. The results of some of these studies suggested that there is a positive correlation between the preferred sites of atherogenesis and the regions of disturbed flow where wall shear stresses are low [12–14]. However, it was not derived from one source but as a combination of several separate results obtained from clinical or postmortem studies and flow studies carried out experimentally by using various models or computer simulations. It is necessary to fill up the gap and put together the separate results of previous clinical or postmortem studies and flow studies mentioned above. Therefore we have prepared pressure-fixed transparent human aortic trees containing the whole heart and nine major branches and studied both flow patterns and preferred sites of atherosclerotic lesions in the abdominal aorta. The present work is an extension of our previous studies in which flow patterns at some branching sites of the dog aortic arch and the abdominal aorta [15,16], and the human aortic arch [11] were investigated, and focuses on the relationship between detailed flow patterns at each branching site of the four major arteries of the thoracico-abdominal aorta and precise locations of atherosclerotic lesions formed in the vessel.

2. Materials and methods

Four isolated transparent human aortic trees containing the whole heart and nine major branches of the aortic tree (brachio-cephalic artery, left common carotid artery, left subclavian artery, celiac artery, superior mesenteric artery, left and right renal arteries, left and right-common iliac arteries) that were used to study flow patterns in the aortic arch [11] were reused in the present study. Observations of preferred sites of atherosclerotic lesions were also carried out on 32 aortas including the ones used for the flow study.

Methods of the flow study, experimental procedures and analysis were all the same as those explained in detail previously [11,15,17,18]. Briefly, the aortic tree that was rendered transparent was placed in a glass chamber filled with methyl salicylate (the same liquid as that was used to render the vessel transparent). A very dilute suspension of a mixture of 50, 80, 115, 230 and 330 μm -diameter polystyrene microspheres in methyl salicylate containing ethanol at 5% by volume used as a substitute for blood was then subjected to steady flow through the aortic tree. The behavior of tracer particles flowing through the abdominal aorta was observed through a zoom-lens system attached to a cine-camera, and photographed on 16 mm cine-films at film speeds from 500 to 1,000 frames per second. The developed 16 mm cine-films were subsequently projected onto a drafting table, and the movements of individual tracer particles were analyzed frame by frame with the aid of a stop-motion 16 mm movie analyzer to obtain detailed flow patterns and distributions of fluid velocity and wall shear rate (shear stress).

In deciding the distribution of the flow from the heart to each branch of the descending aorta, we first checked whether the disturbance in flow that was generated at the aortic arch still remained further down in the area of the abdominal aorta. There we found that the disturbance in the flow had faded away long before the flow reached the branching site of the celiac artery, and velocity profiles were flattened. Therefore we assumed that it would not make any difference to the flow pattern in the abdominal aorta if we closed the three branches of the aortic arch and carried out flow experiments without flow to them.

The actual flow rate in the thoracic aorta, Q_o , was set to 2,600–3,200 ml/min, giving an inflow Reynolds number, $Re_o = D_o \bar{U} \rho / \mu = 1,600\text{--}2,000$, where D_o and \bar{U} were respectively the diameter of the thoracic aorta and mean fluid velocity in the thoracic aorta evaluated just proximal to the branching site of the celiac artery; ρ and μ are the density (1.16 gm/cm³) and viscosity (2.6 mPa s) of the fluid.

Here the cross-sectional shape of the aorta was not circular but elliptical. Therefore, the diameter of the vessel was calculated regarding the shape of the cross-section as an ellipse and taking a mean value of the length of the major and the minor axes.

Regarding the distribution of flow to the branches at a bifurcation, according to Murray [19], it is ideal to distribute the flow from the parent to their daughter vessels in proportion to the cube of their diameters, $Q \propto d^3$. Therefore, we had previously tested the applicability of Murray's law ($D_o^3 = d_1^3 + d_2^3$) to various branching sites of the dog and human aortas and human cerebral arteries. There we encountered a difficulty in deciding the locations at which to measure the diameters of daughter vessels since they decreased gradually after bifurcating, an example of which can be seen in the photographs of the aortas in Fig. 1 of our present paper. Thus, we could not confirm the applicability of Murray's law.

Apart from this, we have carried out our own experimental studies on flow patterns in models of branching vessels using glass-made T-junctions with various branching angles and diameter ratios [20]. There, we found that the critical Reynolds number, Re_c , for the formation of a recirculation flow in the side tube is a maximum around the geometric flow rate ratio, that is, when flow is distributed to the two daughter vessels in proportion to their cross-sectional areas, the flow disturbance in the side tube is at a minimum. Based on this, we considered that the geometric flow rate ratio is an ideal condition in flow distribution at bifurcations. Since then we have been using the geometric flow rate ratio ($Q \propto d^2$) as a standard value for flow distribution to branches in all our flow experiments.

We adopted the same method as described above in our present study, and the flow rate in each branch was set approximately equal to its geometric flow rate ratio (flow rate ratio assumed that fluid from the parent vessel is distributed to the daughter vessels in proportion to their cross-sectional areas assessed at the apex of the flow divider). The actual fractions of the flow (expressed in terms of Q_i/Q_o) that entered each of the six major branches of the descending aorta were approximately 0.25 for both the celiac and superior mesenteric arteries, 0.15 for both the left and right renal arteries, and 0.10 for both the left and right common iliac arteries. For the purpose of presenting flow patterns and velocity profiles at each branching site in the figures, flow conditions specific only to that particular branching site are shown. Representative geometric and flow conditions, D_o , Q_o , \bar{U} and Re_o , were evaluated at the inlet of each section. As in previous studies, flow was visualized and filmed from two different directions in order to deduce the three-dimensional flow patterns and distributions of axial fluid velocity and wall shear stress. Details of the methodology used to compute velocity distributions and wall shear stress are given in the Appendix of the preceding paper on the Aortic Arch [11].

Here, we know that both the flow rate in the aorta and the flow rate ratio between the aorta and side branches vary in response to the change in the physiologic state. For example, during strenuous exercise, the heart increases its cardiac output, and the flow rate in the common iliac arteries increases markedly at

the expense of a drastic reduction of flow rate in arteries feeding the viscera [21]. Such a change in flow rate in the aorta and its branches might affect the flow patterns at each branching site of the abdominal aorta. Therefore we have studied the effects of flow rate, expressed in terms Re_0 , and branch-to-trunk flow rate ratio on the extent of the flow disturbance at the branching site of the renal arteries. The extent of the disturbance was quantified by measuring the axial length of the adverse flow that formed adjacent to the lateral and posterior walls of the abdominal aorta from the flow divider of the left renal artery.

3. Results

3.1. Anatomical structure of the abdominal aorta

Figure 1 shows photographs of several abdominal aortas taken after being rendered transparent. These show that the celiac and superior mesenteric arteries branched off the aorta at the ridge of the anterior wall. Regarding the renal arteries, there were two types, as classified by the anatomical location of the orifice of the two arteries, that is, the anterior-branching type as shown in panels (a), (b), (e) and (f), and the lateral-branching type as shown in panels (c) and (d). The number of the lateral-branching types was

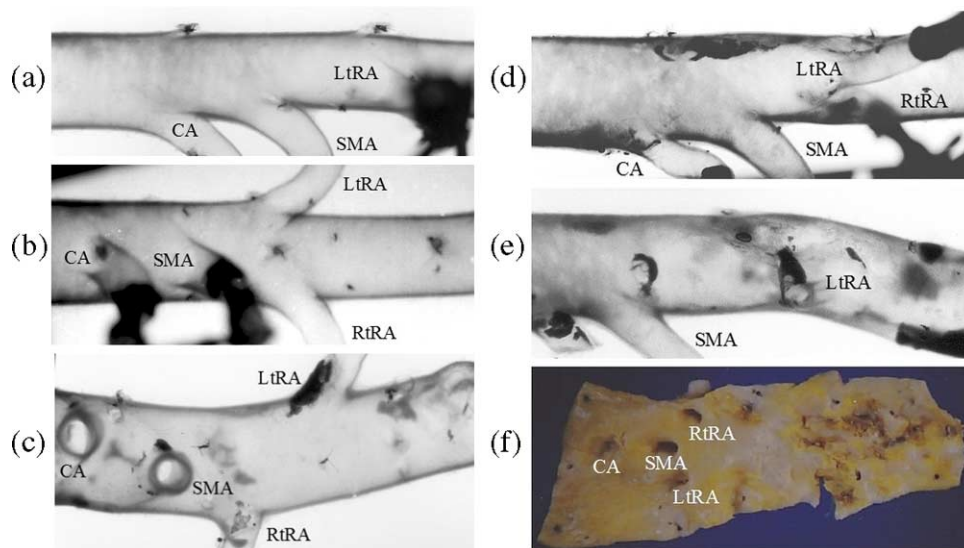


Fig. 1. (a)–(e) Photographs of human abdominal aortas pressure-fixed and rendered transparent, showing the geometric structure of vessels. (a) Lateral view, (b) frontal view of proximal segment from 45-year female showing a stepwise reduction in aortic diameter distal to the branching sites of the celiac (CA) and superior mesenteric arteries (SMA), gentle rounding of the outer wall at each of 4 major branches but very sharp curvature of wall at flow divider. (c) Frontal view of proximal segment from a 68-year-old female subject, development of atherosclerotic lesions with an aneurysmal change on left lateral wall of infra-renal aorta, formation of calcified plaque on proximal lip of orifice of left renal artery (LtRA). Note: infra-renal abdominal aorta is bent towards the left. (d) Lateral view, proximal abdominal segment from a 52-year male showing formation of atherosclerotic plaques on posterior wall opposite orifice of the superior mesenteric artery (SMA) and the anterior wall of the infra-renal abdominal aorta. Note both LtRA and RtRA branch off lateral walls of aorta. (e) Lateral view, proximal segment from 61-year-old male showing the formation of calcified plaques on posterior wall opposite the SMA orifice and anterior wall of infra-renal abdominal aorta and also at sites of branching. Note that infra-renal abdominal aorta is bent anteriorly. (f) The dorsal wall cut longitudinally and opened abdominal segment from 57-year-old male showing typical localization of atherosclerotic lesions in the infra-renal abdominal aorta. Note that the antero-lateral wall within a few cm distal to renal arteries orifices was spared of atherosclerotic lesions. (Colors are visible in the online version of the article; <http://dx.doi.org/10.3233/BIR-14006>.)

somewhat greater than that of the anterior-branching types. However, our classification was not so strict. There were variations in the branching pattern of the renal artery such that in one vessel, the right renal artery emanated anteriorly, while the left renal artery emanated laterally, and vice versa.

The intervals between the branches of the human abdominal aorta were generally shorter than those of the dog that we studied previously [15]. In most cases, the orifice of the right renal artery was located almost at the same level as that of the left renal artery. The flow divider at each branch was sharp and protruded slightly into the oncoming flow, resulting in a stepwise reduction in aortic diameter as shown in panels (a) and (d). The vessel wall opposite the flow divider (the proximal lip of the orifice of the branch) was gently rounded as shown in panels (a) to (e). With aging and the development of atherosclerotic lesions, the geometry of the vessel tended to become modified and the branching angle became dulled as shown in panel (c), and the abdominal aorta became tortuous as shown in panels (c) and (e).

3.2. Preferred sites of atherosclerotic lesions

Twenty-seven aortas (71%) had atherosclerotic lesions on the posterior and lateral walls of the proximal abdominal aorta, corresponding to the branching sites of the celiac and superior mesenteric arteries as shown in panels d and e. By contrast, there were much fewer lesions on the anterior wall except the regions around the orifice of the branches. In middle to distal portions of the abdominal aorta, there were two patterns in topographical distribution of atherosclerotic lesions: (i) Atherosclerotic lesions spread over the abdominal aorta except the anterior wall 3–4 cm from the orifices of the renal arteries as shown in Fig. 1, panel (f) (18 aortas, 50%); and (ii) Atherosclerotic lesions spread over the abdominal aorta except both the left and right lateral walls 3–4 cm from the orifices of the renal arteries (9 aortas, 25%). In both patterns, there were scattered atherosclerotic lesions in regions 3–4 cm distal to the orifices of the renal arteries. There were two other cases that had severe and extensive lesions in the abdominal aorta. They were eliminated from this statistical study. One of them developed an aneurysm as shown in Fig. 2. In this case, the whole infra-renal aorta was affected with atherosclerosis and severely ulcerated. In regions around the orifice of the celiac and superior mesenteric arteries, the proximal lip was affected frequently as shown in panel (d). By contrast, at the orifice of the renal arteries, not only the proximal lip but also the flow divider was affected in some cases.

3.3. Flow patterns in the abdominal aorta

We did flow experiments with all the 4 transparent aortic trees that we used in our previous study on flow patterns in the aorta. There we found that, although the exact nature of the flow differed from vessel to vessel due to variations in the intervals between the four major branches of the abdominal aorta and their branching pattern, in general the flow patterns were qualitatively the same. Thus, they were characterized by the formation of a pair of fan-shaped separation zones adjacent to the lateral walls at each junction and a recirculation zone at the posterior wall from the superior mesenteric artery to distal to the renal arteries. Given the similarity in flow patterns as well as the very laborious and painstaking nature of the work involved in film analysis and preparation of drawings, we have chosen one vessel that we considered the best model prepared in the present study judging by its configuration and good transparency of the vessel wall, and analyzed the films that recorded the flow.

Figures 3(a) and (b) respectively show the flow pattern represented by particle paths and the velocity distribution in the proximal part of the abdominal aorta shown in panels (a) and (b) of Fig. 1 that was

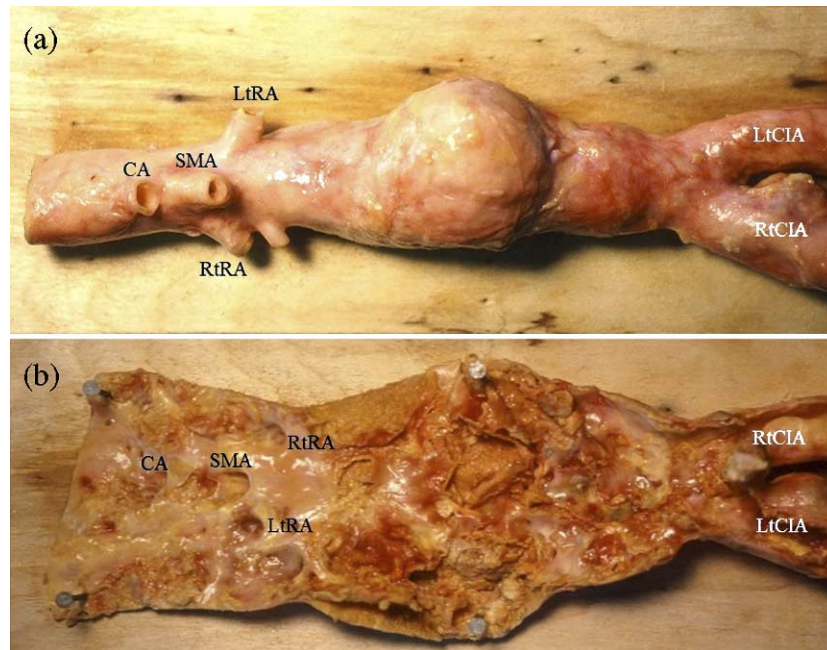


Fig. 2. Photographs of human abdominal aorta with an aneurysm obtained from 72-year-old male. (a) External appearance of abdominal aorta. (b) Luminal surface of the abdominal aorta after being cut longitudinally and opened. Note that whole the infra-renal aorta was affected with atherosclerosis and severely ulcerated. (Colors are visible in the online version of the article; <http://dx.doi.org/10.3233/BIR-14006>.)

prepared from a 21-year-old male subject. Observation was made from left to right, that is, normal to the common median plane of the aorta and the celiac and superior mesenteric arteries.

The particles on streamlines located close to the common median plane traveled almost parallel to the vessel wall and straight through the proximal part of the abdominal aorta as shown by the solid lines. Then the particles on the anterior part of streamlines directly entered the celiac and superior mesenteric arteries and formed the mainstream in these branches. Flow separation occurred at the proximal lip of the orifice of each branch at the point indicated by the letter S in Fig. 3(a). The particles on the central and posterior parts of streamlines slightly shifted their directions towards the anterior wall after passing by these branches. Due to that, flow separation occurred at the posterior wall opposite the flow divider of the superior mesenteric artery as shown by the letter S in Fig. 3(a).

At the aorto-celiac artery junction, the particles on streamlines located in the anterior part and between the common median plane and both the left and right lateral walls (indicated by long-dashed lines) were deflected at the shoulder of the flow divider to both sides of the common median plane. A part of them deflected into the aorta traveled backward along the vessel wall and described arches of various curvatures as shown by the short-dashed lines, and then together with those particles deflected into the branch, entered the celiac artery along the left and right lateral walls wrapping the mainstream of the branch and filled the thin-layered separation zone at the outer wall (opposite the flow divider) of the celiac artery. In this way, a pair of fan-shaped separation zones formed adjacent to the lateral walls at the aorto-celiac artery junction. The rest of the particles traveled forward and entered either the superior mesenteric artery or the abdominal aorta. The particles on streamlines located in the anterior part and located close to the left and right lateral walls gradually moved towards the outer wall (opposite the

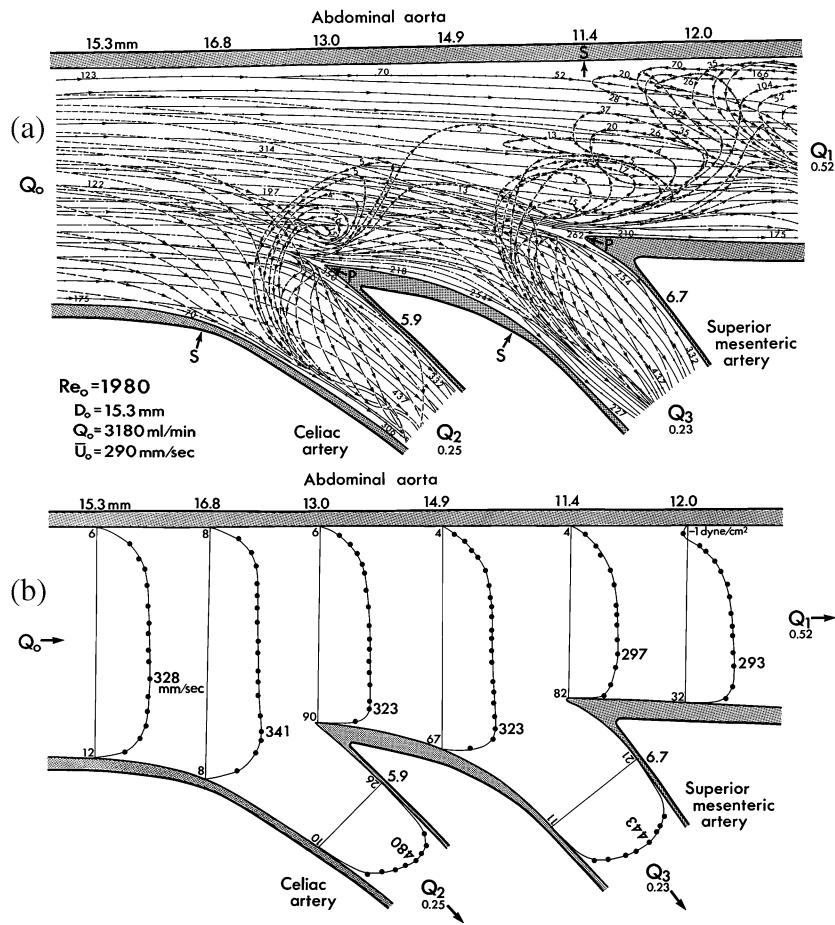


Fig. 3. (a) Detailed flow patterns and (b) distributions of axial fluid velocity and wall shear stress in steady flow in transparent human aortic tree shown in Fig. 1 observed normal to the common median plane of CA and SMA and the aorta (left-lateral view). Drawing constructed by tracing paths of tracer microspheres shows formation of an adverse flow along the dorsal (posterior) wall opposite the flow divider of SMA, and fan-shaped secondary flows at the bilateral shoulders of each junction, and flow separation at the proximal lip of the orifice of each branch. Flat velocity profile at the entrance and then slightly skewed towards anterior wall when passing by flow divider of each branch. Low wall shear stress located along posterior wall and proximal lip of orifice of each branch. Solid lines: paths of particles located in or close to the common median plane; short dashed lines: paths far out of the common median plane; long dashed lines or dash-dotted lines: paths located between the first two types of paths. Arrows at "S" and "P" indicate the points of flow separation and stagnation, respectively. Numbers along the velocity profiles indicate the maximum velocity; numbers at outside and inside of vessels indicate the respective inner diameter and wall shear stress measured at each location. Numbers along the particle paths in (a) indicate particle translational velocities in mm/sec at positions shown. Q_i ($i \geq 1$): ratio of flow rate in aorta and branches to the inflow rate (Q_0). Parameters assessed at inlet of the aortic segment. Re_0 : Reynolds number, D_0 : vessel diameter, Q_0 : volume flow rate, \bar{U}_0 : mean fluid velocity.

flow divider) of the celiac artery and entered the region of separated flow as shown by the curvilinear short-dashed lines. As a result of combination of these different streams shown by the movements of tracer particles, a pair of spiral secondary flows formed in the branch.

A similar flow was observed at the aorto-superior mesenteric artery junction. A pair of deflection flows occurred at the flow divider of the superior mesenteric artery. The particles in the deflected flow traveled slowly along either the left or right lateral wall of the aorta, and a part of them that described small arches changed their directions and traveled backwards along the lateral walls in the same manner as it occurred

at the aorto-celiac artery junction. They then gradually traveled towards the proximal lip of the orifice of the superior mesenteric artery, and after describing arches of various curvatures entered the separation zone formed along the outer wall of the superior mesenteric artery together with the particles traveling slowly near the lateral walls and those particles deflected forward at the flow divider of the celiac artery as described above. Thus a pair of fan-shaped separation zones similar to that formed at the aorto-celiac artery junction formed at this junction too. The particles that described large arches traveled backward slowly along and towards either the left or right postero-lateral wall. Then, they changed directions again and moved forward along the postero-lateral walls. Finally, they approached the posterior proximal lip of both the left and right renal arteries with gradual acceleration and entered them. The particles deflected forward moved slowly along either the left or right antero-lateral wall and approached the proximal lip of both the left and right renal arteries, and entered them.

Figures 4(a) and 5(a) show detailed flow patterns at the aorto-superior mesenteric and aorto-renal artery junctions observed in the same vessel as shown in Fig. 3. The former was observed from left to right, that is, a sequel scene of Fig. 3(a). The latter was observed from posterior to anterior, that is, parallel to the common median plane of the aorta and the celiac and superior mesenteric arteries. The anatomical structure of this vessel as well as all other vessels studied was that the orifices of the left and right renal arteries were located very closely along the axis of the aortic tree. In this particular vessel, the flow divider of the left renal artery was located a few mm proximal to that of the right renal artery. The orifices of left and right renal arteries were located both on the antero-lateral walls (cf. Fig. 1, panel (b)).

The flow pattern at the branching site of the left and right renal arteries was very complex. It was partly due to an asymmetric arrangement of the two branches, that is, the left renal artery was located only a few mm proximal to the right renal artery.

The particles on streamlines located close to the common median plane of the aorta and the celiac and superior mesenteric arteries (referred to as mainstream) shifted their directions towards the anterior wall after passing by the aorto-superior mesenteric artery junction as shown by the solid lines in Figs 3(a) and 4(a) due to that the orifices of both the left and right renal arteries were located on the antero-lateral walls. Then the particles in the mainstream split into the left and right lateral parts and entered the left and right renal arteries, respectively. At the same time, flow separation occurred at the posterior proximal lip of the orifice of both the left and right renal arteries as shown in Figs 4(a) and 5(a). This made the separation zone formed adjacent to the posterior wall at the level of the aorto-superior mesenteric artery junction larger and thicker as it got closer to the aorto-renal artery junctions and all the three separation zones were connected with each other, forming a large recirculation zone. As a result, the separation zone along the posterior aortic wall appeared in the shape of a diamond with its upstream apex locating at the level of the aorto-superior mesenteric artery junction (shown by the letter S in Figs 3(a) and 4(a)). The downstream apex was located well downstream of the aorto-renal artery junctions where the streams reflected at the flow divider of the two renal arteries got together on the common median plane as observed from the posterior to the anterior (Fig. 5(a)). The mainstream in the aorta became very thin and was confined to a narrow region along the anterior wall close to the common median plane at the junctions of the left and right renal arteries with the aorta.

At the entry of each renal artery, particles on streamlines somewhat far from the mainstream were deflected either into the artery or the aorta at the flow divider as shown by the dashed curvilinear lines in Fig. 5(a). The former formed spiral secondary flows in each renal artery. The latter traveled slowly towards the posterior wall along either the right or left lateral wall, encircling the mainstream in the aorta. Then, most of them flowed back slowly and described arches of various curvatures. The particles that described small arches along each lateral wall changed their directions and entered the region of

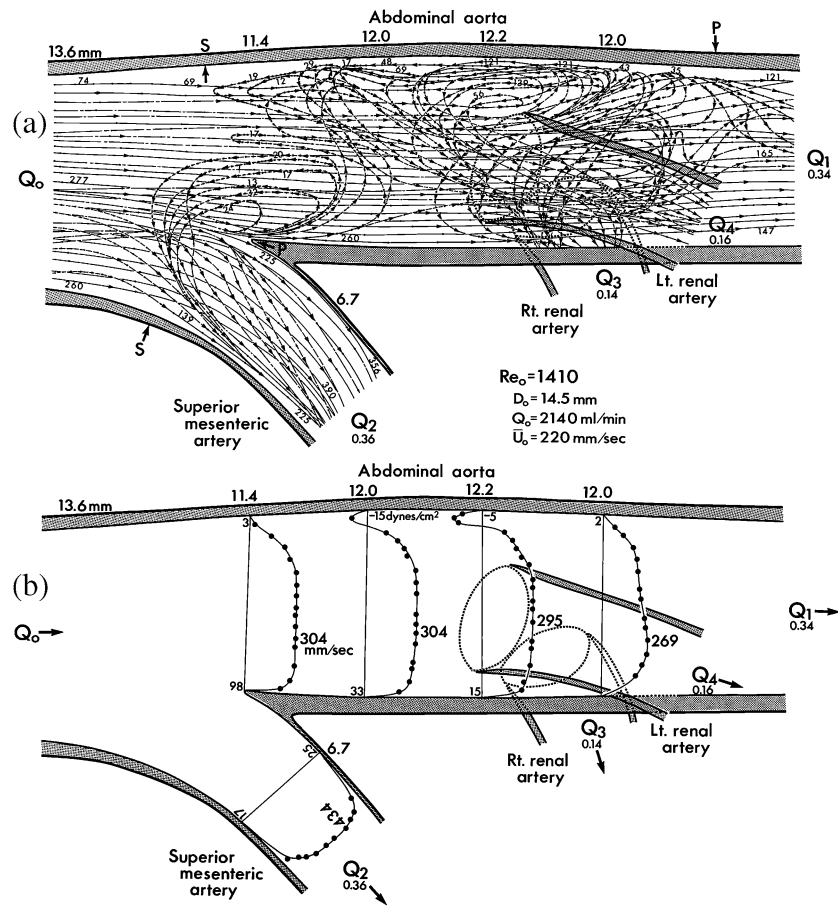


Fig. 4. (a) Detailed flow patterns and (b) distributions of axial fluid velocity and wall shear stress as in Fig. 3 in a left-lateral view containing the bilateral aorto-renal artery junctions. Shown is the formation of fan-shaped secondary flows at the bilateral shoulders of the aorto-superior mesenteric artery junction and a large and long recirculation zone along the posterior and lateral walls around the aorto-renal artery junctions. Velocity distributions show an adverse flow along the posterior wall and skewing of the velocity profile towards the anterior wall. Note: wall shear stress at the posterior wall much lower than that at anterior wall. Arrows at “S” and “P” indicate the point of flow separation and stagnation, respectively.

separated flow formed at the outer wall of each branch. Some of the particles that described relatively large arches moved slowly backward along the posterior wall (dashed lines in Fig. 5(a), solid lines in Fig. 4(a)) up to the point of flow separation (indicated by the letter S in Fig. 4(a)) that occurred opposite the flow divider of the superior mesenteric artery. They then changed directions again and traveled forward along both the left and right lateral walls and entered the renal arteries together with the particles deflected forward at the flow divider of the superior mesenteric artery as shown by the dashed lines in Figs 4(a) and 5(a).

The particles that described arches of large curvature along the left and right lateral walls got together on the distal posterior wall at the point P indicated in Fig. 4(a). Then they trailed along the posterior wall of the infra-renal aorta as shown in Fig. 5(a).

The particles that described arches of intermediate curvature along the left lateral wall crossed the centerline of the posterior wall after traveling along the left postero-lateral wall. They then slowly climbed up the right posterior wall towards the postero-proximal lip of the orifice of the right renal

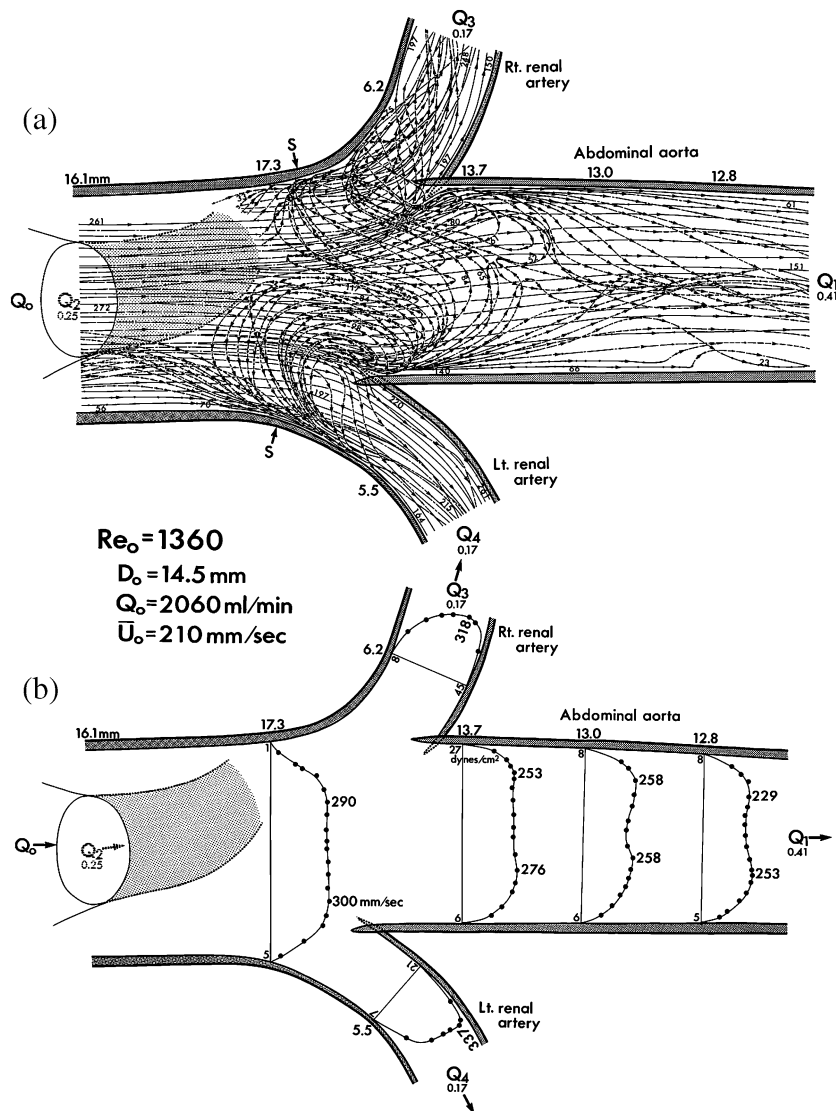


Fig. 5. (a) Detailed flow patterns and (b) distributions of axial fluid velocity and wall shear stress as in Fig. 3 of flow in an abdominal segment containing the bilateral aorto-renal artery junctions viewed normal to the median plane (posterior–anterior view). Shown is the recirculation zone consisting of fan-shaped secondary flows at the aorto-renal artery junctions. Note: part of the secondary flows at the aorto-left renal artery junction enters the right renal artery after describing sigmoid orbits. Velocity profiles are flattened with a local minimum at the center of the vessel in the infra-renal aorta. Regions of low wall shear stress are located at the proximal lip of the orifice of each branch. Arrows at “S” and “P” indicate points of flow separation and stagnation, respectively.

artery. Finally, they entered the artery together with those particles deflected at the flow divider of the right renal artery and with those deflected forward at the flow divider of the superior mesenteric artery as shown in Fig. 5(a). The sigmoid pattern of particle paths observed at the junctions of the left and right renal arteries with the aorta resulted from the particular arrangement of the two branches that the orifice (flow divider) of the left renal artery was located slightly proximal to that of the right renal artery.

The particles on the posterior part of streamlines and located close to the common median plane were directly drawn into the thick-layered separation zone as shown by the solid lines in Fig. 4(a). They then joined the recirculation flow formed by the deflection of flows at the flow divider of each renal artery, as stated above (solid lines in Fig. 4(a), dashed lines in Fig. 5(a)). Finally, they entered either the left or right renal artery.

Figure 6(a) shows a detailed flow pattern at the aorto-superior mesenteric and aorto-renal artery junctions observed in a lateral-branching type vessel. In this vessel, the interval between the superior mesenteric artery and both the left and right renal arteries was very short and the orifice of both the left and

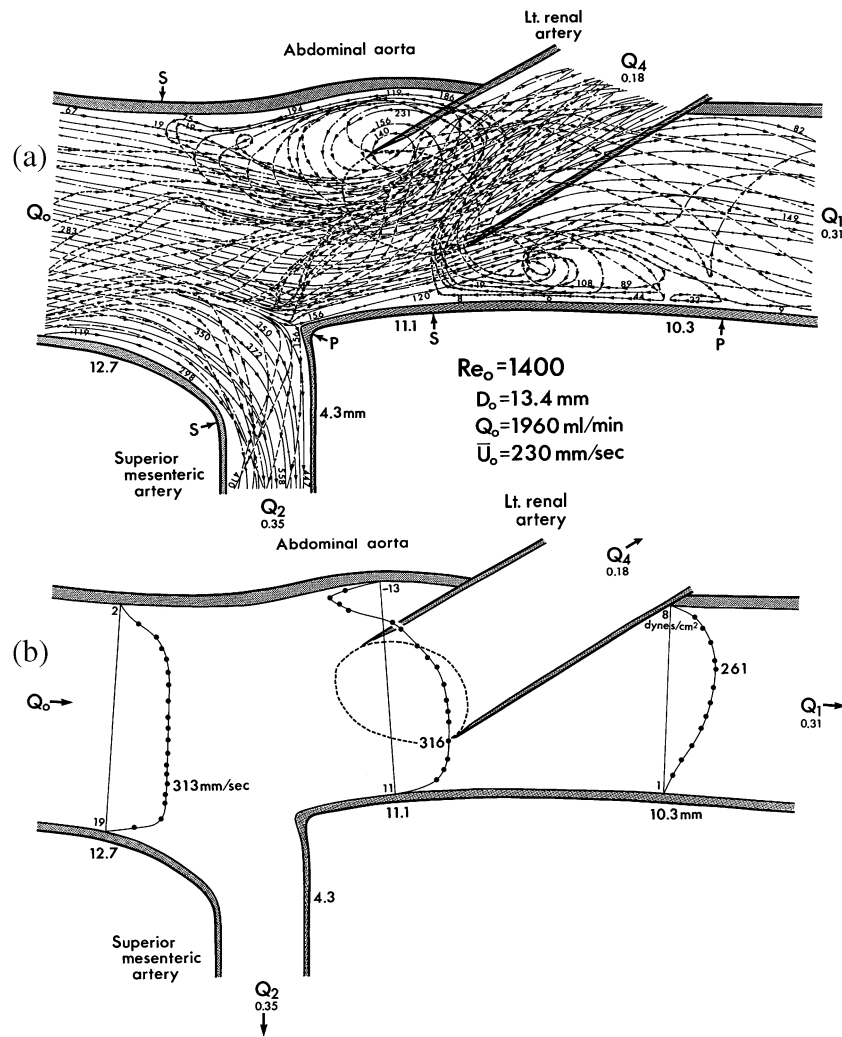


Fig. 6. (a) Detailed flow patterns and (b) distributions of axial fluid velocity and wall shear stress, as in Fig. 3, of flow in an abdominal segment containing the bilateral aorto-renal artery junctions, from a 43-year-old female subject in which the orifice of both left and right renal arteries was located at the same level and on the lateral wall (left lateral view). Shown is a recirculation zone not only along the posterior but also the anterior wall. Note: the velocity of adverse flow in the recirculation zone along the posterior wall is as high as the maximum velocity in the main forward flow, creating region of high wall shear stress. Arrows at "S" and "P" indicate the points of flow separation and stagnation, respectively.

right renal arteries was located at the same level and on lateral wall. The flow was observed from left to right.

Due to the particular anatomical structure described above, most of the particles that were deflected at the flow divider of the superior mesenteric artery directly entered the left and right renal arteries, and no recirculation flow formed along the lateral walls at the aorto-superior mesenteric artery junction.

The particles on streamlines located close to the common median plane shifted their directions towards the anterior wall on approaching the aorto-superior mesenteric artery junction. They then shifted again towards the posterior wall after passing by the flow divider of the superior mesenteric artery. As a result, flow separation occurred at both the posterior and anterior walls at the point indicated by the letter S in Fig. 6(a).

After passing by the aorto-superior mesenteric artery junction, the particles in both the left and right lateral parts of the mainstream in the aorta entered the left and right renal artery, respectively, and formed the mainstream in that artery. As a result, the mainstream in the aorta was confined to a small and thin central core of the abdominal aorta.

The particles on streamlines slightly away from the mainstream of the left and right renal arteries were deflected at the flow divider of each renal artery and entered either the artery or the infra-renal aorta. The latter traveled along the anterior aortic wall as well as the posterior aortic wall and flowed back in the same manner as it occurred in the case of the anterior-branching type vessel shown in Fig. 4(a). As a result, a recirculation zone formed along both the anterior as well as the posterior walls, as shown in Fig. 6(a).

3.4. Distributions of axial fluid velocity and wall shear stress

Figures 3(b), 4(b) and 5(b) show the distributions of axial fluid velocity (axial component of fluid velocity) and wall shear stress in the common median plane (Figs 3(b) and 4(b)) and in the diametrical plane normal to the common median plane (Fig. 5(b)) of an anterior-branching type vessel shown in Fig. 1, panels (a) and (b) and Fig. 3. As shown in Fig. 3(b), the velocity distribution at the entrance of the proximal abdominal aorta was blunted. Then it was gradually skewed toward the anterior wall while going down to the celiac and the superior mesenteric arteries. Thus, the shear stress at the posterior wall was much lower than that at the anterior wall. It was very high around the flow divider of each branch but low at the proximal lip of the orifice of both the celiac and superior mesenteric arteries due to the larger aortic diameter, as shown in Fig. 3(b).

When the flow approached the aorto-renal artery junctions, even greater skewing of the velocity distribution occurred in the anterior-branching type vessel as shown in Fig. 4(b). The shear stress at the posterior wall decreased to even below zero but the absolute value increased momentarily. After passing by the aorto-renal artery junctions, the value of wall shear stress changed from negative to zero and then positive but the absolute value decreased again.

The velocity distributions in the diametrical plane normal to the common median plane of the aorta were skewed towards both the right and left antero-lateral walls, resulting in the formation of bipolar-shaped profiles at and downstream of the aorto-renal artery junctions as shown in Fig. 5(b). Due to a sudden expansion of the aortic diameter proximal to the flow dividers of the left and right renal arteries, the proximal lip of the orifice of the renal arteries was exposed to low wall shear stress.

Figure 6(b) shows the distributions of axial fluid velocity and wall shear stress at the aorto-renal artery junctions in the lateral-branching type vessel. The wall around the flow divider of the superior mesenteric artery and the anterior wall were exposed to low shear stress. By contrast, it was higher at the posterior wall corresponding to the aorto-renal artery junctions due to the formation of a fast recirculation flow.

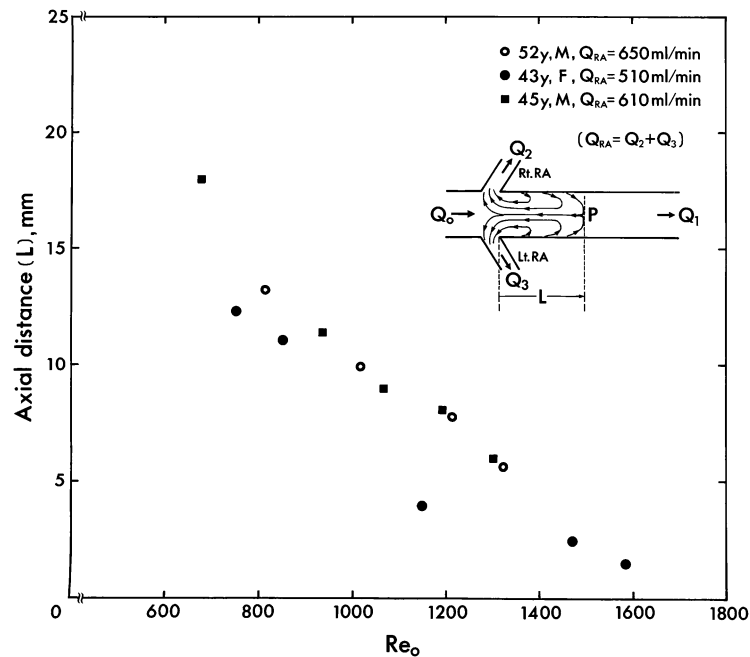


Fig. 7. Plot of the axial length, L , of a recirculation zone measured from flow the divider of the left renal artery against inflow Re_o , assessed in the abdominal aorta proximal to the orifice of the right renal artery, under physiological flow conditions while keeping the flow rate in the renal arteries constant. Flow rates in both renal arteries were kept approximately equal. *Note:* recirculation zone length decreases with increasing Re_o . Shown in the inset is a schematic representation of particle paths in the recirculation zone.

3.5. Effect of flow rate on the size of the recirculation zone

As mentioned above, during a strenuous exercise, the flow rate in the common iliac arteries increases markedly, while the flow rate in arteries feeding the viscera decreases drastically [21]. Therefore, we have studied the effect of flow rate on the extent of the disturbed flow at the branching site of the renal arteries under a constant visceral (especially renal) flow rate using three aortic trees in which the two renal arteries branched off approximately at the same level. It was found that as shown in Fig. 7, the size of the large and long recirculation zone formed along the lateral and posterior walls of the abdominal aorta drastically decreased with increasing Reynolds number (flow rate) as the flow rate in the renal arteries was kept constant.

4. Discussion

The aim of the present study was to investigate the relationship between flow patterns and preferred sites of atherosclerotic lesions formed in the human abdominal aorta. To this end, we first carried out experiments to obtain detailed flow patterns in aortic trees in which no atherosclerotic lesions had yet developed. Then, we studied the relationship between the flow patterns obtained and the preferred sites of atherosclerotic lesions as observed in vessels in which such lesions had developed. By doing so, we could also compare the flow patterns in the human aortic trees with those previously obtained in the dog [15].

It was found that under the conditions of steady flow that simulated the flow in mid-systole, the flow at the entrance of the human abdominal aorta was not fully developed and the velocity profile was flattened as previously found in the dog abdominal aorta [15]. Also, the flow patterns at the aorto-celiac artery and aorto-superior mesenteric artery junctions in the human aorta were similar to those in the dog abdominal aorta [15] but less disturbed even at higher Reynolds numbers. It appears this was due to the particular anatomical structure of the human abdominal aorta in that the aortic diameter decreased stepwise after each branch, with the flow divider at each branching artery sharpened, and with the proximal lip of the orifice of each branching artery gently rounded. As a result, the size of the flow-separation zone and the degree of flow disturbance at these junctions were minimized. However, since the intervals between the junctions of the 4 major branches were much shorter than those in the dog aortas, there were marked interactions between the disturbed flows formed at each junction. In particular, since in most vessels the orifices of the renal arteries were very close to the orifice of the superior mesenteric artery, and since the orifices of both the left and right renal arteries were located almost at the same level, the flow-separation zone at the junction of the superior mesenteric artery extended to the junctions of the renal arteries. Furthermore, due to the particular arrangement of two renal arteries so that they were not located perfectly symmetrically with respect to the common median plane of the aorta and the celiac and superior mesenteric arteries as in the case of the arterial model used by Moore et al. [12–14] and Taylor et al. [22,23], there occurred a cross flow from the left to the right across the common median plane as demonstrated by the sigmoid pattern of particle paths shown in Fig. 5(a). As a result, a large recirculation zone formed along the posterior aortic wall between the aorto-superior mesenteric artery and the aorto-renal artery junctions as shown in Figs 4(a) and 6(a). In many vessels, atherosclerotic lesions and plaques were found at this site as shown in Fig. 1, panel (d).

However, the precise sites and sizes of the atherosclerotic lesions and plaques found in vessels used for the study of the preferred sites of these lesions did not necessarily coincide with those of the recirculation zone and the region of low wall shear stress formed in the vessel used to study flow patterns. For example, in the vessel shown in Fig. 1, panel (d), the head of the atherosclerotic plaque formed at the posterior wall is located at the level of the celiac artery (CA), a point that is more proximal to the separation point of the recirculation zone formed in the vessel shown in Fig. 1, panel (a) (also Fig. 1, panel (b), Figs 3 and 4), and the size of the atherosclerotic plaque is much larger than that of the recirculation zone. Here, the differences between the two vessels are that the diameter of the aorta shown in Fig. 1, panel (d) is much larger than that shown in Fig. 1, panel (a), and the flow divider of the CA protrudes less into the oncoming flow than in the vessel shown in Fig. 1, panel (a). This will result in much lower wall shear stress at the anterior wall in the vessel shown in Fig. 1, panel (d) than that in the vessel shown in Fig. 1, panel (a) (cf., Figs 3 and 4). Furthermore, in the vessel shown in Fig. 1, panel (d), the renal arteries are located laterally, while in the aorta shown in Fig. 1, panel (a), they are located anteriorly. In the aorta shown in Fig. 1, panel (a) (cf., Figs 3 and 4), the separation point (head of the recirculation zone) is located opposite the orifice of the superior mesenteric artery (SMA), while in the aorta shown in Fig. 6, it is located proximal to the orifice of the SMA. In this way, although the general flow pattern is the same, the exact nature of the flow is different from one vessel to another. Thus, the apparent discrepancies in the location and size of the atherosclerotic plaque formed in the vessel shown in Fig. 1, panel (d) and the location and size of the recirculation zone formed in the vessel shown in Fig. 1, panel (a) (cf., Figs 3 and 4) could be accounted for by the differences in the geometry of the vessel and the arrangement of the orifices of the branches. It is very likely that in the case of the vessel shown in Fig. 1, panel (d), flow separation occurred at a point located more proximally than in the case of the vessel shown in Fig. 1, panel (a) (cf., Figs 3 and 4), and the plaque was formed at the very site where a recirculation flow formed.

Unfortunately, we did not try flow experiments with this vessel due to the poor clarity of the vessel and the presence of many raised plaques that may cause a disturbance of the flow. Nevertheless, there was a certain difference in the precise sites of atherosclerotic lesions between the anterior-branching and the lateral-branching type aorta as determined by the anatomical locations of the orifices of the renal arteries.

In the anterior-branching type aortas, the mainstream in the aorta was very thin and confined to a narrow region along the anterior wall close to the common median plane at the junctions of the left and right renal arteries. Due to that, the wall shear stress in the infra-renal aorta was higher on the anterior wall than the posterior and lateral walls. This might be related to the finding that a narrow area of the anterior wall within a few cm from the orifices of the renal arteries was frequently spared from atherosclerotic lesions (cf., Fig. 1, panel (f)). In the lateral-branching type aortas, the mainstream was located at the center of the abdominal aorta through the four major branches, and a recirculation zone formed along both the posterior and anterior walls (Fig. 6(a)). A statistical study on the topographic distribution of sudanophilic lesions in the human aorta carried out by Cornhill et al. [2] as well as the results of our present study indicated that both the posterior and anterior walls of the infra-renal aorta were frequently affected by atherosclerosis, while the lateral walls were spared. Another study carried out by Nguyen and Haque [24] also showed that the frequency of plaque formation in the abdominal aorta was high at the posterior and anterior inferior walls, and the inflow tracts of the four major branches. It appears that the distribution of atherosclerotic lesions in the infra-renal aorta is greatly affected by the branching pattern of the renal arteries.

As shown in Fig. 1, panel (c), among the aortic trees we studied, some had a branching pattern similar to that of the dog aorta, that is, the orifice of the right renal artery was located further distally to that of the left renal artery. In such a vessel, atherosclerotic lesions were localized exclusively at the proximal lip of the orifice of the left renal artery and the left posterior aortic wall at the left renal artery. This might be also related to the particular flow pattern that a fan-shaped separation zone (recirculation flow) formed along the left lateral and posterior walls at this site as shown in our previous paper [15].

Studies on the effects of hemodynamic factors such as the flow velocity and flow division at sites of branching on flow patterns and wall shear stress have been carried out by many investigators [25–27]. Mostbeck et al. [25] performed velocity-encoded cine magnetic resonance imaging at five different levels of the abdominal aorta in nine healthy volunteers, and showed that net retrograde flow (expressed as a percentage of antegrade flow) increased from proximal to distal levels and was maximal just distal to the origin of the renal arteries. They stated that the location of retrograde flow they detected *in vivo* in the abdominal aorta was close to that obtained with *in vitro* flow-visualization studies carried out with models of the human abdominal aorta.

Ku et al. [26] and Moore et al. [13] characterized flow patterns in a glass model of the human abdominal aorta that included its major branches. In this model, the orifice of both the celiac and superior mesenteric arteries was located at the anterior wall and the orifice of both the left and right renal arteries was located at the lateral walls. Therefore the model they used corresponded to the lateral-branching type aorta studied in our present work. They carried out experiments under the 3 different conditions, resting, exercise, and postprandial conditions, and visualized flow patterns in both steady and pulsatile flows by injecting green and red dyes. Their results showed that under the resting conditions, two vortices formed at the level of the orifices of the renal arteries. One formed on the anterior wall and another one that was larger than the first one formed on the posterior wall in both steady and pulsatile flows. Under the postprandial conditions that were simulated by a 90% increase in flow rate in the superior mesenteric artery, a vortex and a reverse flow formed, respectively, on the anterior wall and along the posterior wall

in the same time sequence as the resting conditions, and an additional region of oscillatory flow formed along the anterior wall approximately halfway between the superior and inferior mesenteric arteries. Under the exercise conditions that was simulated by a drastic reduction of the flow in the celiac, superior mesenteric, and renal arteries to increase the flow in both the left and right common iliac arteries to 80% of the total inflow, flow became laminar and orderly throughout the infrarenal aorta, and no turbulence nor other high-frequency disturbances were observed. Their findings that under the rest and postprandial conditions, vortices formed on the anterior wall and along the posterior wall agree well with our results obtained in the lateral-branching type aortas (cf., Fig. 6(a)). The results that the vortices disappeared under the exercise conditions also agree with ours that the size of the recirculation zone decreased and eventually disappeared with the increase in flow rate in the common iliac arteries.

Studies on flow patterns in the abdominal aorta were also carried out by means of computational fluid dynamics (CFD). Taylor et al. [22,23] simulated the blood flow in a model of the normal human abdominal aorta that was the same as that used by Moore et al. [12–14] (lateral branching type aorta) in pulsatile flow under resting conditions, and obtained flow patterns and wall shear stress. They showed that a recirculation zone formed along the posterior wall of the infrarenal aorta. Regions of low time-averaged wall shear stress and high shear-stress temporal oscillations were located in this region along the posterior wall of the infrarenal aorta opposite the orifice of the superior mesenteric artery and along the anterior wall between the superior and inferior mesenteric arteries. These regions coincided with the regions of a high probability-of-occurrence of sudanophilic lesions reported by Cornhill et al. [2]. They also showed that under the simulated moderate exercise conditions, all the regions of low wall shear stress and high oscillatory shear index were eliminated. Tang et al. [27] carried out a similar study by using subject-specific models of the human abdominal aorta constructed from magnetic resonance angiograms of five young, healthy subjects. They showed that under exercise that was simulated by 50% increase in resting heart rate, wall shear stress (WSS) increased more than 6 fold, while oscillatory shear index (OSI) decreased to 1/10 of the value obtained at rest at the supraceliac, infrarenal, and suprabifurcation levels, and there was a significant difference in WSS between the anterior and posterior sections.

The results described above all suggest that physical fitness that increases the flow rate in the lower limbs mitigates flow disturbance and minimizes the region of low wall shear stress in the abdominal aorta, resulting in lower incidence of the development of atherosclerotic lesions. By contrast, a sedentary life that reduces the flow in the lower limbs and enhances flow disturbances in the abdominal aorta might promote the development of atherosclerotic lesions as suggested by Zarins [5]. In fact, it was shown in animal studies carried out with pigs that physical fitness inhibited the development of atherosclerotic lesions in the pig abdominal aorta [28]. This might be related to the flow modification observed in our study.

Regarding the preferred sites of atherogenesis, Moore et al. [14] studied the relationship between the wall shear stress obtained in a glass model of the human abdominal aorta and the sites of intimal thickening obtained from postmortem human aortas. They showed that the posterior wall of the infrarenal aorta where time-averaged mean wall shear stress was the lowest coincided with the locations of maximal intimal thickening. In contrast to this, pulse and maximum shear stresses did not correlate with plaque localization. They concluded that in the infrarenal aorta, regions of low mean and oscillating shear stress are predisposed to the development of atherosclerotic plaques while regions of relatively high wall shear stress tend to be spared. These results also agree with our finding that preferred sites of atherosclerotic lesions were localized exclusively in regions where flow was disturbed by the formation of secondary and recirculation flows and where wall shear stress was low.

In our present study, we did not try flow experiments under pulsatile flow. However, since the results obtained in our present study are very much the same as those obtained by all the investigators described above, we consider that the results we obtained under the condition of steady flow that simulated mid systole fairly well reflected the physiological phenomena related to localized genesis and development of atherosclerotic lesions in the human abdominal aorta.

In summary, we have studied the relationship between flow patterns and preferred sites of atherosclerotic lesions in the human abdominal aorta and found that in both the anterior-branching type and lateral-branching type vessels, atherosclerotic lesions developed selectively in regions of recirculation flows where flow was very slow and wall shear stress very low.

Acknowledgements

This work was carried out while the authors were working in the McGill University Medical Clinic at the Montreal General Hospital, Montreal, Canada, and it was supported by Grant HL-41187 awarded to Dr. Karino from the National Heart, Lung and Blood Institute, National Institute of Health (USA). The authors thank the late Dr. W.P. Duguid of the Department of Pathology at the Montreal General Hospital for his help in obtaining human aortas at autopsy.

References

- [1] Caro CG, Fitz-Gerald JM, Schroter RC. Arterial wall shear and distribution of early atheroma in man. *Nature*. 1969;223:1159–61.
- [2] Cornhill JF, Herderick EE, Stary HC. Topography of human aortic sudanophilic lesions. *Monogr Atheroscler*. 1990;15:13–9.
- [3] Schwartz CJ, Mitchell JRA. Observations on localization of arterial plaques. *Circ Res*. 1962;11:63–73.
- [4] Svindland A, Walløe L. Distribution pattern of sudanophilic plaques in the descending thoracic and proximal abdominal human aorta. *Atheroscler*. 1985;57:219–24.
- [5] Zarins CK, Glagov S. Pathophysiology of human atherosclerosis. In: Wilson SE, Veith FJ, Hobson RW, Williams RA, editors. *Vascular surgery – principles and practice*. New York: McGraw-Hill Book Company; 1987. p. 23–41 (Chapter 3).
- [6] DeSanctis RW, Doroghazi PM, Austen G, Buckley MJ. Medical progress – aortic dissection. *New Eng J Med*. 1987;317:1060–7.
- [7] Schlatmann TJ, Becker AE. Histologic changes in the normal aging aorta: implication for dissecting aortic aneurysm. *Am J Cardiol*. 1977;39:13–20.
- [8] Slater EE, DeSanctis RW. The clinical recognition of dissecting aortic aneurysm. *Am J Med*. 1976;60:625–33.
- [9] Zarins CK, Glagov S, Vesselinovitch D, Wissler RW. Aneurysmal formation in experimental atherosclerosis: relationship to plaque evolution. *J Vasc Surg*. 1990;12:246–56.
- [10] DeBakey ME, Gerald ML, Glaeser DH. Patterns of atherosclerosis and their surgical significance. *Ann Surg*. 1985;201:115–31.
- [11] Endo S, Goldsmith Karino T HL. Flow patterns and preferred sites of atherosclerotic lesions in the human aorta - I. Aortic arch. *Biorheology*. 2014;51:239–55.
- [12] Moore JE Jr, Ku C, Ku DN. Pulsatile velocity measurements in a model of the human abdominal aorta under resting conditions. *J Biomech Eng*. 1994;116:337–46.
- [13] Moore JE Jr, Ku DN, Zarins CK, Glagov S. Pulsatile flow visualization in the abdominal aorta under different physiologic conditions: implications for increased susceptibility to atherosclerosis. *J Biomech Eng*. 1992;114:391–8.
- [14] Moore JE Jr, Xu S, Glagov S, Zarins CK, Ku DN. Fluid wall shear stress measurements in a model of the human abdominal aorta: oscillatory behavior and relationship to atherosclerosis. *Atheroscler*. 1994;110:225–40.
- [15] Endo S, Goldsmith HL, Karino T. Flow patterns in the dog descending aorta under a steady flow condition simulating mid-systole. *JSME Intern J Series C*. 2004;47:1000–9.
- [16] Endo S, Sohara Y, Karino T. Flow patterns in the dog aortic arch under a steady flow condition simulating mid-systole. *Heart Vessels*. 1996;11:180–91.

- [17] Asakura T, Karino T. Flow patterns and spatial distributions of atherosclerotic lesions in human coronary arteries. *Circ Res.* 1990;66:1045–66.
- [18] Karino T, Motomiya M. Flow visualization in isolated transparent natural blood vessels. *Biorheology.* 1983;20:119–27.
- [19] Murray CD. The physiological principle of minimum work. I. The vascular system and the cost of blood volumes. *Proc Natl Acad Sci USA.* 1926;12:204–14.
- [20] Karino T, Goldsmith HL. Particle flow behavior in models of branching vessels. II. Effects of branching angle and diameter ratio on flow patterns. *Biorheology.* 1985;22:87–104.
- [21] Anderson DL. The cardiovascular system in exercise. In: Falls HB, editor. *Exercise physiology.* New York: Academic Press; 1968. p. 101–7.
- [22] Taylor CA, Hughes TJR, Zarins CK. Finite element modeling of three-dimensional pulsatile flow in the abdominal aorta: relevance to atherosclerosis. *Ann Biomed Eng.* 1998;26:975–87.
- [23] Taylor CA, Hughes TJR, Zarins CK. Effect of exercise on hemodynamic conditions in the abdominal aorta. *J Vasc Surg.* 1999;29:1077–89.
- [24] Nguyen ND, Haque AK. Effect of hemodynamic factors on atherosclerosis in the abdominal aorta. *Atheroscler.* 1990;84:33–9.
- [25] Mostbeck GH, Dulce MC, Caputo GR, Proctor E, Higgins CB. Flow pattern analysis in the abdominal aorta with velocity-encoded cine MR imaging. *J Magn Imag.* 1993;3:617–23.
- [26] Ku DN, Glagov S, Moore JE Jr, Zarins CK. Flow patterns in the abdominal aorta under simulated postprandial and exercise conditions: an experimental study. *J Vasc Surg.* 1989;9:309–16.
- [27] Tang BT, Cheng CP, Draney MT, Wilson NM, Tsao PS, Herfkens RJ, Taylor CA. Abdominal aortic hemodynamics in young healthy adults at rest and during lower limb exercise: quantification using image-based computer modeling. *Am J Physiol Heart Circ Physiol.* 2006;291:H668–76.
- [28] Link RP, Pedersoli WM, Safanie AH. Effect of exercise on development of atherosclerosis in swine. *Adv Exp Med Biol.* 1972;22:127–42.